JOURNAL OF GEOPHYSICAL RESEARCH: ATMOSPHERES, VOL. 118, 1734–1746, doi:10.1029/2012JD017845, 2013

Coordinated investigation of summer time mid-latitude descending E layer (E_s) perturbations using Na lidar, ionosonde, and meteor wind radar observations over Logan, Utah (41.7°N, 111.8°W)

Tao Yuan,[1] C. Fish,[2] J. Sojka,[1] D. Rice,[3] M. J. Taylor,[1] and N. J. Mitchell[4]

Received 26 March 2012; revised 8 November 2012; accepted 25 November 2012; published 28 February 2013.

[1] It is well known that there is a strong correlation between the formation of a descending sporadic E layer (E_s) and the occurrence of large upper atmospheric zonal wind shears, most likely driven by solar thermal tides and/or gravity waves. We present new results of E_s perturbation events captured between 13 and 17 July 2011 (UT days 194–198) as part of a coordinated campaign using a wind/temperature Na lidar at Utah State University [41.7ºN, 111.8°W], and a Canadian Advanced Digital Ionosonde (CADI; Scientific Instrumentation Ltd., Saskatoon, Saskatchewan, Canada) and SkiYMet meteor wind radar, both located at nearby Bear Lake Observatory [41.9°N, 111.4°W]. During this period, the CADI detected strong descending E_s on 2 days (195 and 197) when large modulations of the top-side mesospheric Na layer occurred in synchronism with strong oscillations in the ionosonde E region echoes. A weakening in the descending E layer echoes was observed on the other 2 days (196 and 198) coincident with a large reduction in the zonal diurnal and semidiurnal amplitudes above 95 km. Both tidal components were found to have comparable contributions to the total zonal wind shear that was critical for E_s formation and its downward propagation. Further investigation indicates that the weakening tidal amplitudes and the occurrence of the E_s events were also influenced by a strong quasi-two-day period modulation, suggesting significant quasi-two-day wave (QTDW) interactions with the tides. Indeed, a nonlinear, wave-wave interaction-induced 16-hour period child wave was also detected, with amplitude comparable to that of the prevailing tides. These interaction processes and their associated effects are consistent with earlier Thermosphere Ionosphere Mesosphere Electrodynamics General Circulation Model studies of nonlinear interactions between the migrating tidal waves and the QTDW and were probably responsible for the observed damping of the tidal amplitudes resulting in the disruption of the E_s.

Citation: Yuan, T., C. Fish, J. Sojka, D. Rice, M. J. Taylor, and N. J. Mitchell (2013), Coordinated investigation of summer time mid-latitude descending E layer (E_s) perturbations using Na lidar, ionosonde, and meteor wind radar observations over Logan, Utah (41.7°N, 111.8°W), *J. Geophys. Res. Atmos.*, *118*, 1734–1746, doi:10.1029/2012JD017845.

1. Introduction

[2] Mid-latitude E_s is a compressed plasma sheet found in the lower E region of the ionosphere (90–120 km). It was discovered and has since been studied extensively using remote observations by ionosondes, incoherent scatter radars (ISR), and coherent backscatter radars [e.g., review by *Mathews*, 1998, and the reference within], and more recently using global positioning system (GPS) instrumentation [*Arras et al*., 2009]. Joint resonance fluorescence lidar campaigns with ISR or ionosonde have shown the connection between E_s and sporadic neutral metal layers [*Tepley et al*., 2003; *Raizada et al*., 2011; *Williams et al*., 2007]. The anomalies and irregularities of E_s and its considerable effects on radio wave communications [*Zeng*, 2010 *and Sokolovskiy*, 2010] are of significant importance to scientists from various fields of radio communication, atmosphere, and space sciences, etc. The well-accepted, though still incomplete, theory about tidal ion layer E_s [*Whitehead*, 1989; *Mathews*, 1998, and the references within] states that its formation is driven by a large wind shear that is generated in the upper atmosphere through tidal or gravity wave modulation of the neutral wind. The theory also concludes that E_s evolution requires ion-neutral collisional coupling and geomagnetic Lorentz forcing to initiate a negative vertical

[1]Center of Atmosphere and Space Sciences, Utah State University, Logan, Utah, USA.
[2]Space Dynamic Laboratory, Utah State University Research Foundation, North Logan, Utah, USA.
[3]Space Environment Corporation, Providence, Utah, USA.
[4]Department, Electronic and Electrical Engineering, University of Bath, Bath, UK.

Corresponding author: T. Yuan, Center of Atmosphere and Space Sciences, Utah State University, Logan, Utah, USA. (titus.yuan@usu.edu)

2169-897X/13/2012JD017845

ion convergence that drives the long-lived metal ions into the lower thermosphere. Thus, the formation and propagation of E_s is the direct result of coupling between the neutral atmosphere and the E region ionosphere, and investigations of E_s will greatly assist in the understanding of the coupling between these two regions.

[3] According to the aforementioned wind shear theory, when neglecting diffusion and electric field forcing, the vertical ion drift speed (W) within the E region at mid-latitudes can be approximated as shown in equation (1),

$$W \approx \frac{VcosIsinI + U\gamma cosI}{1+\gamma^2} \quad (1)$$

assuming northward pointing magnetic field lines. Here I is the magnetic dip angle, and γ is the ratio of ion-neutral collision frequency to ion gyrofrequency. In the lower E region below 115 km, the ion-neutral collision frequency is relatively high, with $\gamma >> 1$. Therefore, W is dominated by the zonal wind (U) component and the meridional wind (V) contribution becomes minimal, resulting in $\partial W/\partial z \propto \partial U/\partial z$ (where z is altitude), identifying the important role of the zonal wind in E_s formation. This theory correlates well with the high E_s occurrence rate in the Northern Hemisphere, mid-latitude summertime when the zonal wind shifts fairly quickly from east- to westward within the lower E region, and when solar thermal tidal waves are active, generating a negative vertical zonal wind gradient that is modulated by atmospheric waves. It is also coincident with the incident meteor rate peak that occurs during the summer. Since the E_s contains a high percentage of metallic ions that are generated by the ablation of meteors entering into the thermosphere, it implies that meteor flux may be also another important factor or source in E_s formation [*Haldoupis et al*., 2007].

[4] In the mid-latitude E region, although the diurnal tide amplitude is generally weaker than semidiurnal tides' amplitude, both of which have been proven to be two of the most significant dynamic features [*Forbes*, 1995], with amplitudes greater than a few tens of m/s [*Yuan et al*., 2008a] and increasing rapidly up to ~115 km altitude. It is also suggested that tidal waves may set up the environment for gravity wave (GW) breaking and induce instabilities along with large shears [*Liu*, 2007; *Zhao et al*., 2003; *Li et al*., 2005a, 2005b] in the background wind. Therefore, tidal wave modulation is one of the key sources for inducing/maintaining the large vertical zonal wind shear that is required for mid-latitude E_s formation. Indeed, Na lidar observations had revealed strong correlations on the order of 60% probability of occurrence between large wind shears (>50 m/s/km) and large tidal wave amplitudes [*Yue et al*., 2010]. Tidal and planetary wave activities have been linked to E_s formation in many early studies [*Tong et al*., 1988; *Lanchester et al*., 1991; *Haldoupis and Pancheva*, 2002, 2004; *Voiculescu et al*., 2000]. For example, semidiurnal tidal signatures were found in E_s occurrence rates at higher mid-latitudes using GPS radio occultation measurements [*Arras et al*., 2009].

[5] Although there have been considerable investigations concentrating on the characteristics of mid-latitude E_s, detailed and comprehensive studies of the atmospheres dynamical conditions, especially effects of atmospheric waves, are rare during E_s events, due mainly to the dearth of coincident neutral wind and temperature measurements in the lower E region. The linkage between tidal wave activity and E_s occurrence is postulated mostly based on the occurrence rate and slope of the descending E layer, without direct measurements of temperature and horizontal wind tidal components in the lower E region. Since most of the waves, generated from lower atmospheric sources, ultimately propagate into the lower E region, a diagnostic of these waves' characteristics within the neutral mesopause region is therefore reasonable and critical to understand E_s formation and its evolution. The Na Doppler wind/temperature lidar can obtain neutral temperature and wind information within the mesopause region. It can observe this region during the full diurnal cycle, under clear sky conditions, with the help of Faraday filter technology [*Chen et al*., 1996]. Even though Na lidar cannot directly detect ion irregularities within the whole E region, collaborative observations with an ionosonde can measure the indirect impact on the upper region of the mesospheric Na layer, such as sporadic Na layer [*Williams et al*., 2007]. But, more importantly, lidar can provide key dynamical parameters, including high-resolution neutral temperature and horizontal wind profiles, as well as related tidal and planetary wave information [*Yuan et al*., 2006, 2008a; *She et al*., 2004] within the D region and lower E region f ionosphere. In this article, we study E_s perturbation events captured on 4 nights during a collaborative campaign using a cluster of instruments, including Na lidar, ionosonde, and meteor wind radar (MWR), revealing, for the first time, the correlation between E_s perturbation and tidal/planetary wave variability.

[6] This article has the following outline: In section 2, we describe the instruments involved in this campaign study, including the Na Doppler temperature/wind lidar at the Utah State University (USU) main campus in Logan, Utah, and the Canadian Advanced Digital Ionosonde (CADI; Scientific Instrumentation Ltd., Saskatoon, Saskatchewan, Canada) ionosonde and MWR, both located at the Bear Lake Observatory (BLO) near Garden City, Utah. In section 3, we present the coincident measurements from the three instruments during the July E_s event. In section 4, we describe the tidal and planetary waves' activities revealed by lidar and MWR and discuss their contributions to the total wind shear. Conclusions and summary of this study are provided in section 5.

2. Instruments

[7] The Na lidar facility, complemented by the CADI and MWR at BLO located ~40 km northeast of Logan, Utah, is a narrow band resonance fluorescence Doppler lidar system operating at the Na D_2 line with a 120 MHz full-width half-maximum laser pulse bandwidth. It is the heritage of the Na lidar system developed at Colorado State University, which was relocated to USU in the summer of 2010, after two decades of operation in Colorado. It can provide critical atmospheric information throughout a full diurnal cycle of observations of the mesopause region (80–110 km), weather permitting. The Na lidar is currently set up to probe the mesopause region in three directions (north, east, and west) during the night and in two directions (north and east) during the daytime using a pair of Faraday filters. The lidar operated for 88 hours from 21:40 UT on day 194 to 15:59

UT on day 198 with a small, ~3-hour data gap on day 197, providing continuous temperature, zonal and meridional wind profiles, as well as Na density measurements. Such complete diurnal cycle lidar observations have proven to be essential for studying variations in the mean fields and tidal waves (24-, 12-, 8- and 6-hour) [*She et al.*, 2004] and for establishing climatologies [*Yuan et al.*, 2006, 2008a, 2008b, 2010] for the mid-latitude mesopause region. In this article, hourly binned lidar data, with 2 (night) and 4 km (day) vertical resolutions, are utilized to retrieve the mean fields as well as tidal information. The lower spatial resolution during the daytime was necessary to compensate for the relatively low signal-to-noise ratio of the lidar data while operating under sunlit conditions. The short-period perturbations from atmospheric GW were mostly smoothed out by this hourly averaging approach, while possible long-period gravity wave modulations, such as inertia waves, are stored in the residual terms during the fitting process. Planetary wave effects during the campaign are likely to add a small bias to the mean field values, depending on their periodicity and on the length of campaign measurements.

[8] At BLO, the University of Bath SkiYMet MWR provided continuous horizontal wind measurements throughout the campaign. The MWR is an all-sky interferometric system [*Hocking et al.*, 2001] that employs a high-pulse repetition sounding to detect and measure meteor trail echoes. The MWR transmits continuously at a fixed frequency of 32.5 MHz, with a power output of ~6 kW using a crossed Yagi antenna, and receives on a 5-Yagi (crossed) antenna configuration. Each hour, a horizontal wind vector is fitted to 3 km wide height bins over a sampled height interval of 82–98 km. The MWR meteor trails are detected primarily at mid- to low-elevation angles and represent an average wind over a horizontal region of ~400 km in diameter centered on BLO. Located alongside the MWR, the CADI ionosonde was manufactured by Scientific Instruments Ltd. and operated by the Space Environment Corporation (SEC; Logan, Utah). The CADI's frequency range was 1–20 MHz and height resolution 3 km. As the transmitter power was restricted to 100 W, the daytime operations were often limited by D-region absorption.

3. Observations

3.1. CADI Observation of E_s

[9] The CADI ionosonde measures the ionospheric echo strength every 10 minutes to form a single ionogram. Each E region echo signal is mapped at a specific E-region frequency (f_oE) and a virtual height on the ionogram. The top row in Figure 1 shows 7 ionograms taken at hourly intervals on UT day 197 from 00:00 to 06:00 UT showing the development of E_s. To convert every two-dimensional (2D) ionogram into a one-dimensional (1D) profile so that the E layer vertical structure can be assessed at the time of the measurements, our analysis approach was carefully chosen to comprehensively cover all the ionosphere information. In the example shown here, for each ionogram we mapped each unique pair of echoes altitudes back to the zero f_oE and the interception point with the *y*-axis on the

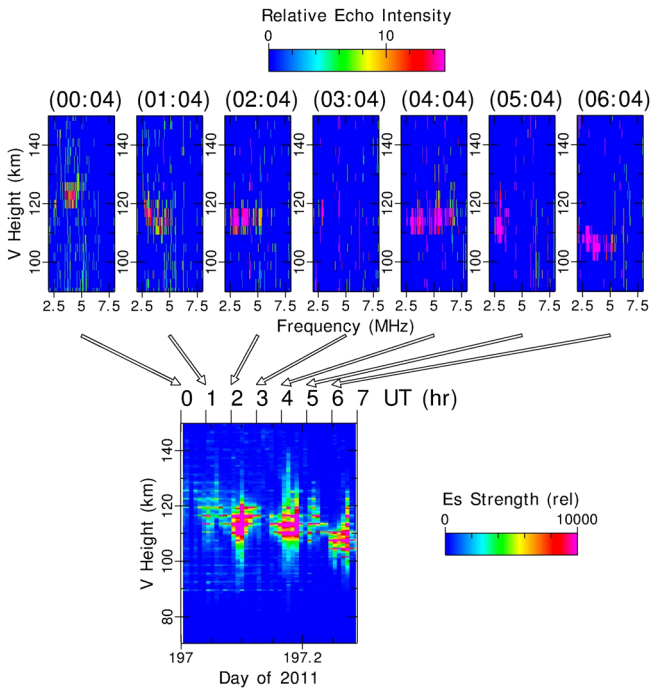

Figure 1. Top panel shows seven CADI ionograms taken at hourly intervals from BLO beginning at 00:04 (hr:min) UT on day 197 in 2011. Each ionogram's relative echo intensity is color coded as shown in the above key. The lower panel shows the results of applying a descending layer fitting process to each ionogram during this 7-hour period. The descending layer intensity is also color coded, as indicated by the key to the right of the panel. Each ionogram is linked to its descending layer time via an arrow.

ionogram provides a new altitude for the pair. The mean value of the two fitted echoes was then assigned to represent a new echo value for this altitude. If all echoes at different f_oE occurred at the same height, then this mapping would correspond to a unique height at zero f_oE. Given that the ionograms typically show a layer thickness of 2–4 range gates spread in altitude, and can have slopes (e.g., Figure 1 ionograms at 01:04 and 06:04 UT), this mapping produces a spread in heights. If a large gradient existed through the f_oE, then our analysis would also be able to capture this feature. Another advantage of this analysis approach is that it will highlight any strong thin E_s layers, since most of the echo values will reside over a small altitude range. The result of this fitting algorithm is the generation of a new vertical distribution of E layer echo strength with randomly spaced intervals for each ionogram. We then bin this new echo profile into 0.5 km intervals. The results of this are shown in the lower panel of Figure 1, which includes information from all of the 42 ionograms between 00:00 and 07:00 UT on day 197, using the above analysis.

[10] This procedure results in a 1D height distribution that favors horizontally bunched echoes that cover a wide frequency spread. In testing, this procedure was found to be more effective in reproducing E_s layers than a simple compaction of all echoes into a 1D altitude distribution at zero f_oE, as shown in the lower panel of Figure 1. In this panel, the altitude distribution of the E_s layer is represented as a color-coded vertical stripe without smoothing in either vertical or horizontal axis. The color represents the weighted echo count in 0.5 km altitude binning. This figure also provides a "calibration" in altitude due to the 3 km range gate resolution of the CADI operation mode. The height distribution is "banded" at 3 km intervals due to the high occurrence of echoes that lie in the same range gate but at different frequencies. For example, in the Figure 1 ionogram at 04:04 UT, the E_s layer is seen as echoes occupying three distinct adjacent range gate intervals. The descending layer is readily identified in Figure 1 (lower panel) after combining all the outputs from the above analysis algorithm between UT 00:00 and UT 07:00 on day 197. However, the plot shows that the "strength" of the descending layer is also modulated in a very clear manner, with a roughly 2-hour periodicity. This aspect of the descending layer may have been caused by a deep penetrating, fast gravity wave modulating the layer during the observation period, which is left to a later study.

[11] The current investigation period covers 5 days over which the Na resonance lidar operated, namely days 194–198 of 2011. During this time, the BLO CADI observed 720 ionograms. Each ionogram was processed in a manner described above to determine the height distribution and strength of any descending layers. The results of this analysis are shown in the top panel of Figure 2. For comparison, the results of Figure 1 are included in the 5-day time plot of Figure 2 at day 197. (Note, the dayside E layer echoes contain a "grid" of faint horizontal lines at 3 km altitude spacing, which is an artifact of this analysis method and should be ignored.) However, the dayside data show a prenoon descending feature that is slightly different each day. A good example of this occurs

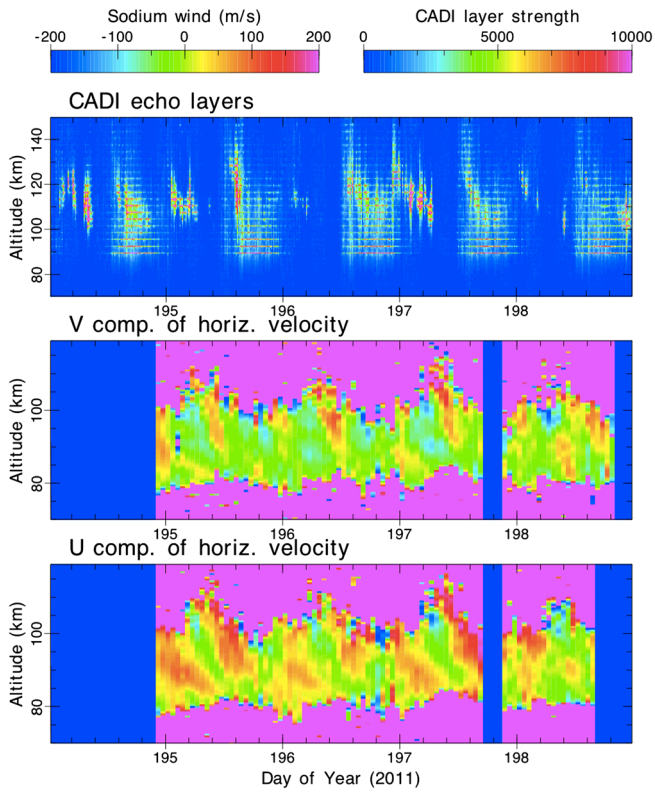

Figure 2. Contour plot of CADI detected Es relative echo strengths (top) from 13–17 July 2011. The middle and lower plots show the corresponding Na lidar measurements of the meridional and zonal winds, respectively.

on UT day 196 at ~12:00 UT when the enhanced layer was at 118 km and descended over the next 6 hours to about 114 km. At ~22:00 UT, a second layer appears at ~130 km before evolving into the nighttime descending layer in the early hours of day 197, as shown in Figure 1.

3.2. Tidal Wave Period Modulations During E_s Event

[12] Figure 2 also shows the simultaneous observations of the meridional (middle) and zonal wind (bottom) as determined from the Na lidar data. At BLO, the approximate start time of the descending layers occurred around 00:00 UT. The ionosonde detected strong E layer irregularities on days 194, 195, and 197, while the echoes on days 196 and 198 were fairly weak. Comparatively, the zonal wind speed and its modulations on the days of strong E_s were considerably larger than on those days with weak E_s, while the meridional wind variations did not exhibit any clear correlation with the occurrence of E_s. The differences in the zonal winds on these nights are clearly visible in Figure 3, which shows the zonal nighttime wind variations from 90 to 110 km, as measured by the lidar. The downward progression of the zonal wind maximum, which indicates upward wave propagation, is clearly visible on days 195 and 197 (when the E region echoes were strong), with a peak to trough difference of over 200 m/s near 105 km. In contrast, on UT days 196 and 198, the wind modulations were weak and less regular, consistent with weaker wave modulations. The CADI data of Figure 2 also show strong E_s on day 194 (prior to the start of the lidar measurements). Further investigation using the MWR wind observations for this day also confirms a strong zonal wind modulation. This suggests that the weakening of E_s on days 196 and 198 was well correlated with weak zonal wind modulations in the lower E region. Since tidal waves are the major driving forces for the large wind shears creating E_s, their behaviors during this campaign merit further investigation.

[13] Near mid-latitudes, the migrating semidiurnal tide is the dominant tidal mode, especially in the lower thermosphere, where it is quite insensitive to background dissipation due to its relatively long vertical wavelength ~45–55 km [*Forbes*, 1995]. Earlier studies have also shown that the lidar observed semidiurnal modulations are dominated by the migrating semidiurnal tidal wave [*Yuan et al.*, 2006, 2008a, 2008b]. In contrast, the migrating diurnal tidal component, albeit the dominant diurnal component, is more sensitive to dissipation and thus is more variable around mid-latitudes [*Yuan et al.*, 2010]. To retrieve tidal components from the continuous lidar observations, a least-square fitting method was applied to the diurnal cycle measurements with durations of 24 hours or greater. We used a constant for the mean ($j = 0$), 24-hour ($j = 1$), 12-hour ($j = 2$), 8-hour ($j = 3$), and 6-hour ($j = 4$) period in the fitting process, as shown in equation (2).

$$\Phi(z,t) = \bar{\Phi} + \sum_{j=1}^{4} A_j(z)\cos\left[\frac{2\pi j}{24}(t-\theta_j)\right] + R(z,t) \qquad (2)$$

[14] Φ can be any of the Na lidar mesopause region measurements (e.g., the zonal or meridional wind or

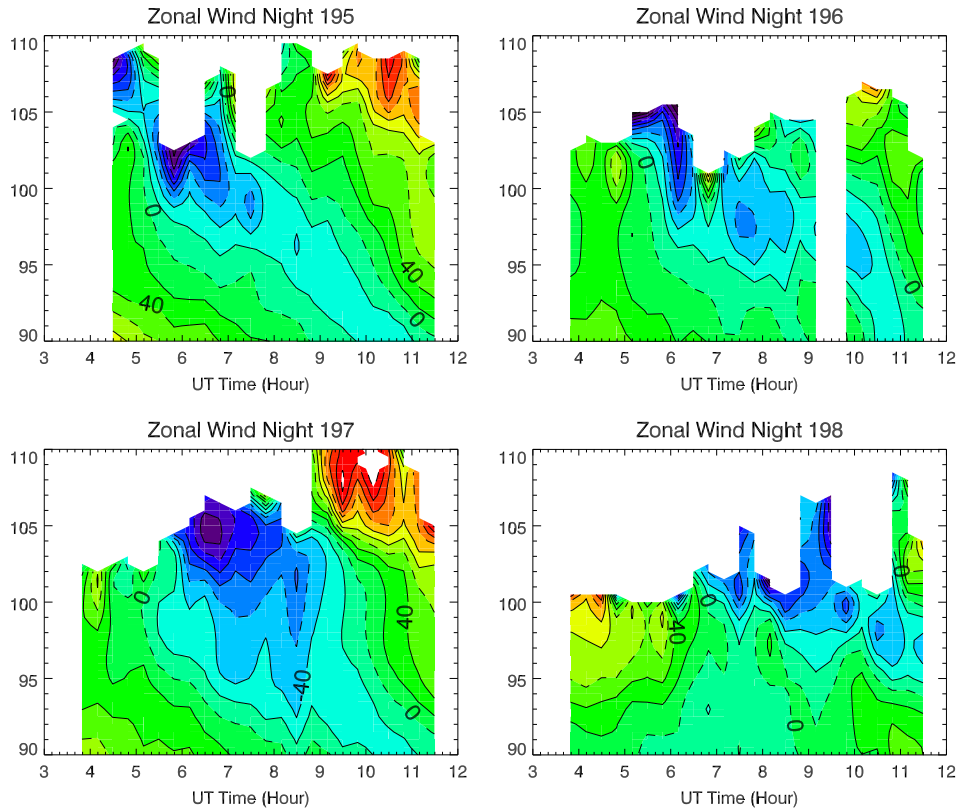

Figure 3. Zonal winds over the altitude range 90–110 km, as measured by the Na lidar during the nights of 195 (top left), 196 (top right), 197 (bottom left), and 198 bottom right).

temperature etc.). For tidal component calculations using multiday, full diurnal cycle observations, the hourly values were sorted according to their local solar time (LST) from 00:00 to 23:00 LST prior to applying the harmonic fit process. Since the zonal wind is a driver of E_s formation, we will focus on this tidal wave component's contribution for the rest of this article.

[15] Figure 4 shows Lomb periodogram analysis for temperature (top left), zonal wind (top right), meridional wind (bottom left), and Na density (bottom right), based on the 4-day total of 88 hours of Na lidar observations. The three contour level lines represent the translated confidence levels of 50% (solid), 95% (dotted), and 99.5% (dashed) from spectrum power [*Yuan et al*., 2006], showing the percentages of the relative signal strength that are unlikely generated by white noise. It is apparent that the semidiurnal components are the most dominant modulations near, and above, 88 km for all four fields with highest power. The diurnal components are the second most prominent, with activity seen mostly below 90 km, except for the zonal wind that exhibits a secondary peak near 98 km. There also appears to be a significant quasi-two-day wave (QTDW) modulation in the zonal winds at ~86 km altitude and in the Na density observations at ~93 km. The appearance of strong 16-hour signals in the zonal wind (90–100 km) and temperature (84–88 km) components was unexpected, as it is not a normal tidal mode. The Na density and meridional wind field of Figure 4 also exhibited signs of such a 16-hour wave near 86 km, which may be due to an inertial GW. Alternatively, model simulations suggest it may also be a "child wave" as a result of nonlinear interactions between the QTDW and migrating tide (diurnal or semidiurnal), that are known to generate intermediary 16-hour period waves [*McCormack et al*., 2010; *Palo et al*., 1999]. The long vertical wavelength of this wave revealed by the lidar measurements suggest the latter mechanism is the major source (this is discussed later in section 4).

[16] Figure 5 shows diurnal (top) and semidiurnal amplitude (middle) variations of the zonal wind between 86 and 98 km throughout the lidar campaign. Each tidal component amplitude and phase values were retrieved by applying the above least-squared fitting method (equation (2)) within a 24-hour window, with a sliding 1-hour step forward throughout the 88 hours of wind measurements. Note, to fill in the small data gap for this moving window tidal calculation, we reconstructed the hourly zonal wind results from UT time 18:00 to 20:00 on day 197 by using the mean and tidal components deduced from the 4-day lidar observation period as proxy components. Since the gap only represents a small portion (~3 hours) of a full day, the deduced tidal results for day 197 should still represent a close approximation to those derived from the complete 24-hour data sets. Figure 5b confirms the dominance of the semidiurnal tidal modulation over the diurnal modulation. The plot also reveals that the semidiurnal component incurred significant damping on days 196 and 198, especially on day 198 when its amplitude was

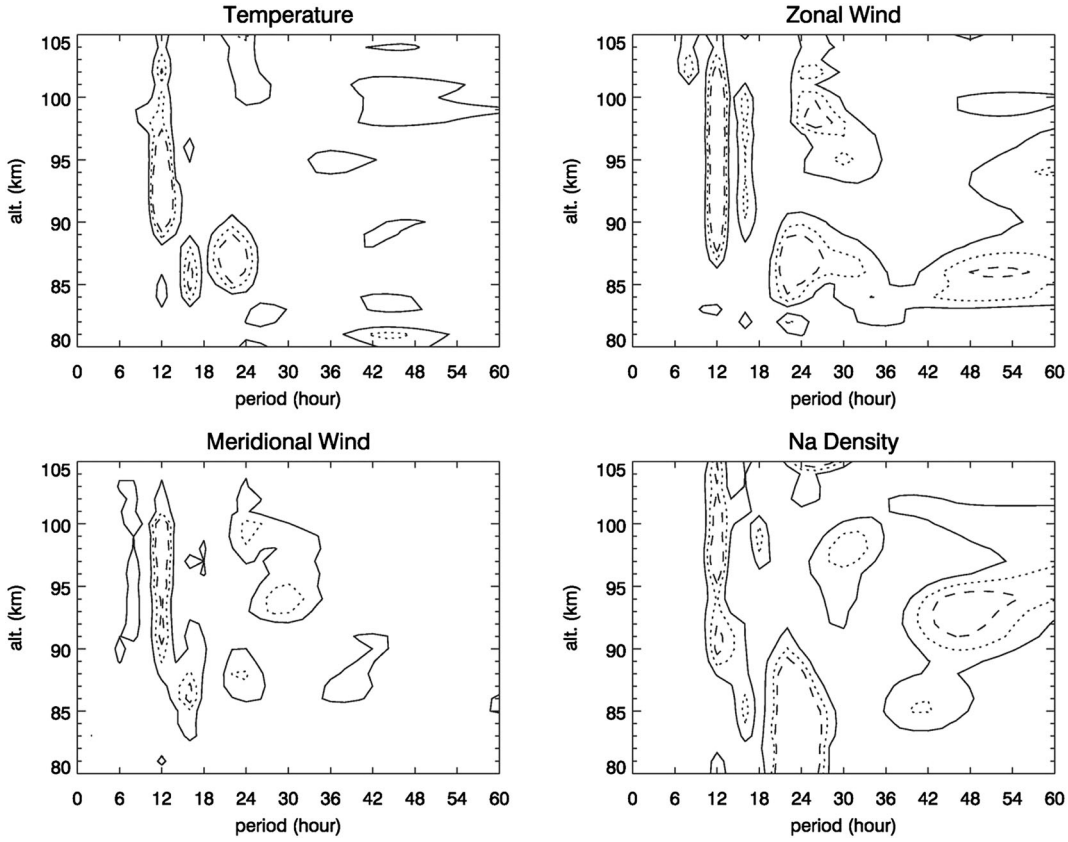

Figure 4. Lomb periodogram analysis based on full diurnal cycle Na lidar measurements of temperature (top left), zonal wind (top right), meridional wind (bottom left), and Na density. The contour lines label 50% (solid line), 90% (dotted line), and 95% (dashed line) statistics confidence levels of wave signatures.

reduced to ~30 m/s near 95 km, while it was over 60 m/s on days 195 and 197, at the same altitude. The diurnal amplitude above 92 km shows similar variations with relatively strong amplitude (~30 m/s around 95 km), but less than 20 m/s on the other 2 days. A further investigation of diurnal and semidiurnal phases indicates that they were continuously downward progressing within the mesopause region on the 2 nights (195 and 197) when strong E_s occurred (but their upward energy propagation was disturbed on the 2 nights with weak E_s echoes). In addition, when the residual of the tidal harmonic fitting (raw lidar wind data minus tidal reconstructed wind (as was utilized to fill the small data gap on day 197) was fitted with a 16-hour wave using a sliding 16-hour window, the wave amplitude (Figure 5c) shows a comparable magnitude to the semidiurnal tide in Figure 5b and was much stronger than the diurnal component on day 197. On day 195, the 16-hour wave's amplitude (>40 m/s near 96 km) was also larger than the diurnal amplitude, but was much less than the semidiurnal tidal component. Its amplitude was much smaller on days 196 and 198 when the weak E_s occurred.

[17] To investigate the QTDW's role during this period, continuous wind observations that have much longer temporal coverage than the lidar campaign are essential. Fortunately, the nearby MWR at BLO was operating during this period. Due to its continuous day/night and weatherproof operation, planetary and tidal wave information on the zonal wind can be fully derived from these data. The MWR observations also provide a more complete picture of the zonal wind tidal variations on the last day of the lidar campaign (day 198), which was only revealed partially by the lidar measurements (Figure 5). Figure 6 shows the 48-hour wave (QTDW) amplitude variation (top) from days 194 to 199, encompassing the lidar operations. This was determined by using a sliding 2-day least-square fitting method applied to the MWR zonal wind measurements from days 191 to 201 at 3-hour intervals. The time series of 24- (middle) and 12-hour amplitude variations (bottom) were calculated using equation (2) and the same fitting procedure applied to the same lidar data set, but using a sliding 1-day window with a 1-hour step size, to achieve the same time resolution as the lidar results. For the majority of the data, the root mean square residual variance (>90%) indicates that the fitting uncertainties for 85 and 94 km were small and less than 7.5 and 10 m/s with standard deviation of mean wind less than 4 m/s, respectively, indicating a good fit between the model and experimental data. The upper panel of Figure 6 depicts considerable variability in the amplitude and structure of the QTDW during this period. Initially, the QTDW appeared to be trapped mainly below 90 km prior to day 195. Throughout most of day 196, the QTDW amplitude increased (to over 20 m/s near 88 km) and also exhibited a secondary peak near 94 km. Thereafter, the 2-day wave's amplitude weakened markedly (end of day 196/first half of 197). By the middle of day 198, the QTDW's

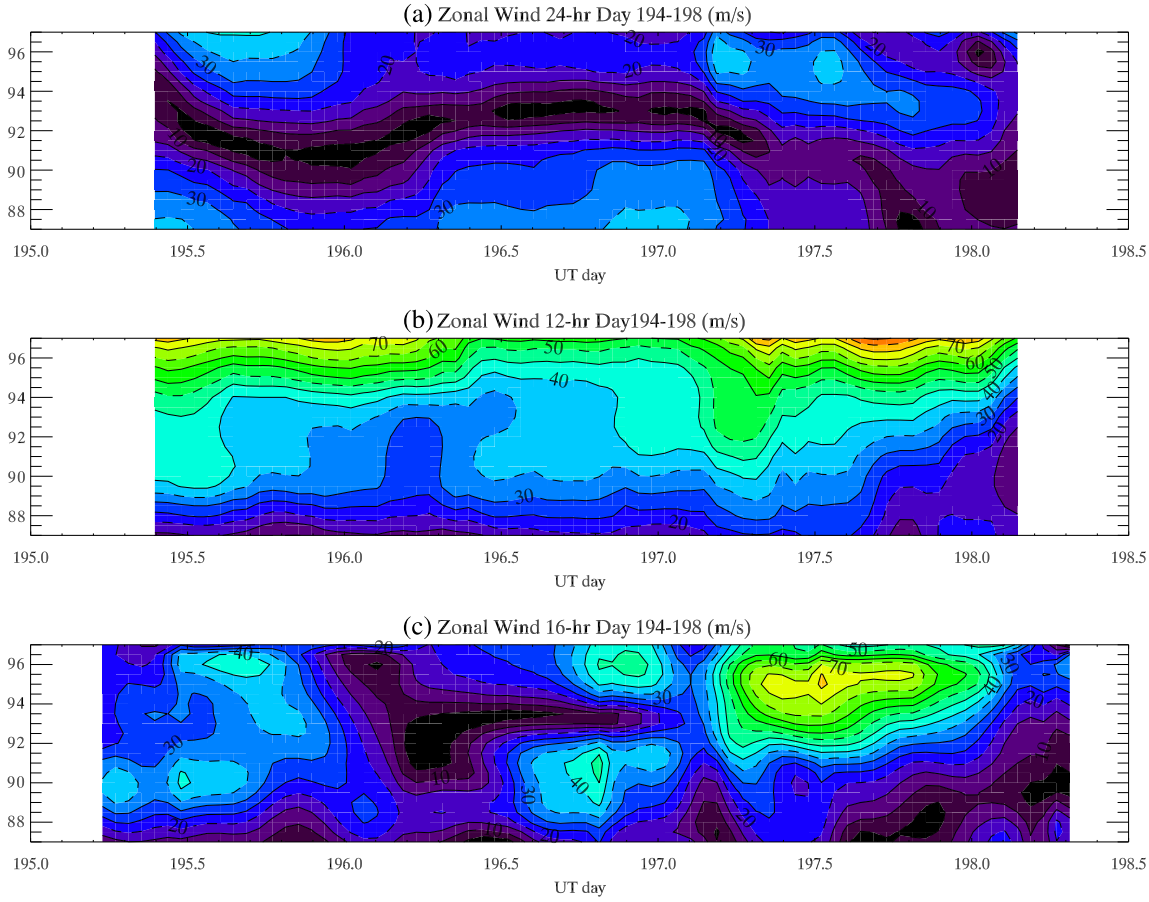

Figure 5. Time series analysis of (a) zonal wind diurnal amplitude, (b) semidiurnal amplitude, and (c) the 16-hour wave measured by the Na lidar from days 195 to 198.

amplitude had reached a maximum of over 25 m/s and exhibited a well-defined double-peaked structure with a primary peak below 86 km and a secondary peak centered near 95 km with similar amplitude. QTDW's exhibiting such a double-peaked feature was also well documented in an earlier modeling study by *Palo et al*. [1999]. For comparison, the MWR diurnal and semidiurnal tidal amplitudes (Figure 6, middle and lower panels) show variations similar to those of the lidar measurements (Figure 5) and further confirm that both tidal components underwent significant damping during day 198, when the weakest E_s occurred. Importantly, although the diurnal amplitudes from both instruments are similar in magnitude, the MWR's semidiurnal amplitudes appear to be considerably smaller in magnitude than those observed by the lidar. Calibration of the BLO MWR and USU lidar measurements will be presented in a later article.

3.3. Disturbance in Top Side of Na Layer During E_s

[18] The major reservoir species for atomic Na above 96 km is Na^+, and its conversion to neutral atoms (which involves quenching species, N_2, H_2O, and O, as well as e^-) is known to be slightly anticorrelated with in situ neutral temperature [*Plane et al*., 1999]. Thus, extra injection of electrons and Na^+ by the descending E layer will inevitably change the chemical interaction rates within the top side of the mesospheric Na layer. Figure 7 shows a time series of nocturnal Na column abundance over the altitude range 105–120 km for the four consecutive nights of lidar Na observations (days 195–198). The measurements are denoted by the asterisks where the uncertainty in the Na density measurements was $<10^8/m^3$. For comparison, the CADI measurements of peak electron density (dotted lines) and relative echo strength (dashed lines) are also plotted. (Note the relative echo strength data have been increased by 5.0×10^{10} to accommodate them on the same plot.) It is clear that during the E_s events (on days 195 and 197 from 04:00 to 07:00 UT), the topside Na abundance experienced considerable variation in synchronization with the E_s perturbations. Following the cessation of the E layer echoes, the oscillations in the top-side Na abundance also stropped and were replaced by a smoothly varying curve on both of these nights. Furthermore, although the Na column abundances during the second half of the nights were of similar magnitude for all 4 nights, during the first half of night, it was clearly much higher on days 195 and 197 when E_s was present. The CADI E layer signal was also weakest on the night of 198, with a peak electron density below

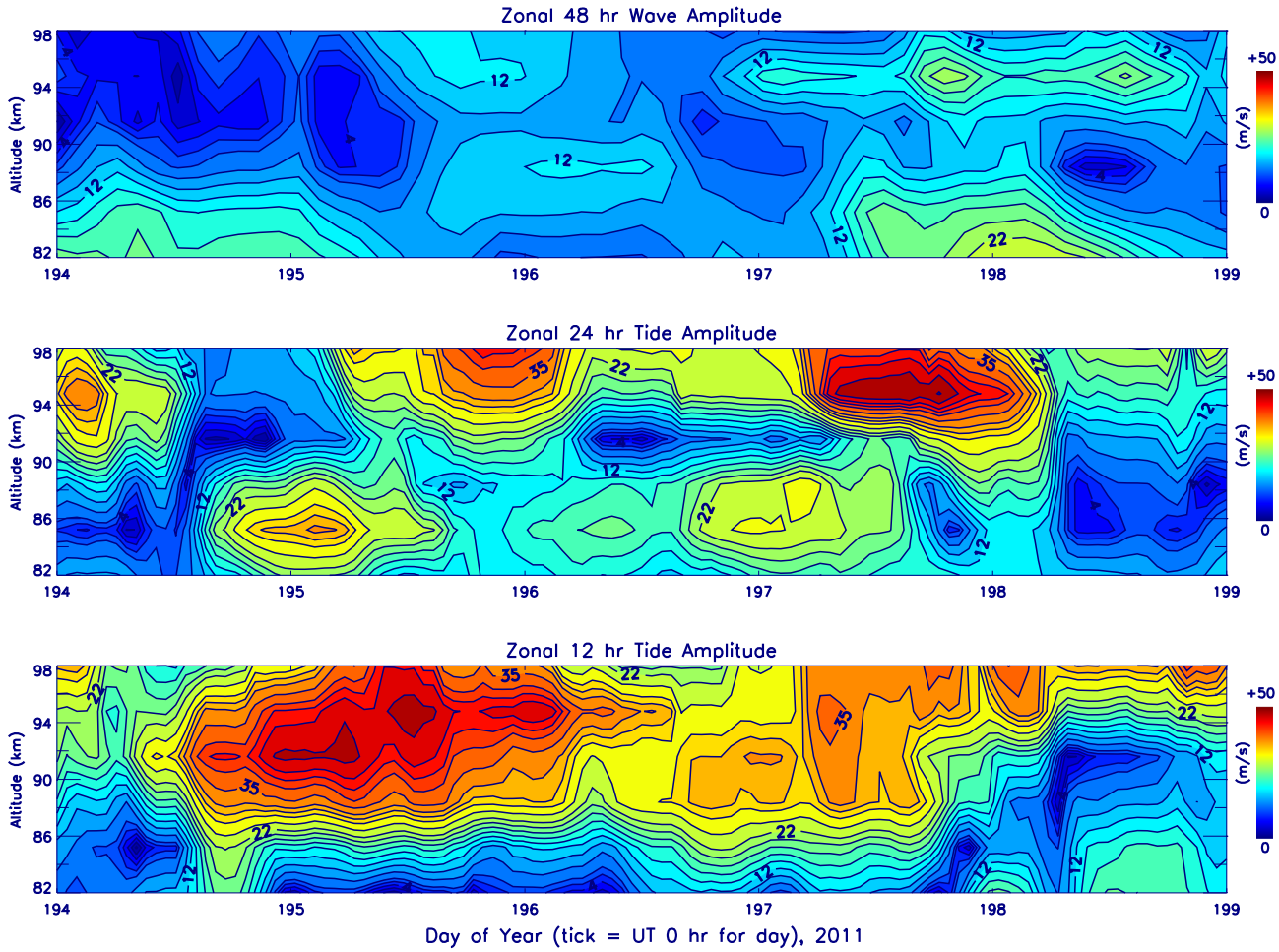

Figure 6. Time series of MWR observations of zonal wind QTDW (top), diurnal (middle), and semidiurnal tidal wave (bottom) amplitudes from days 194 to 198. The tick marks on the horizontal axis represent UT time 00:00 for each day.

$10^{10}/m^3$, associated with the lowest top-side Na abundance of the four nights ($<10^{10}/m^2$). The Na lidar also detected sporadic Na layers above 105 km in all three directions during the E_s (not shown), but they appeared at slightly different local times, with the strongest Na echoes arising from the east beam, suggesting the propagation of a horizontally inhomogeneous E_s layer.

[19] In summary, the Na abundances were significantly higher on the nights with strong E_s than those with weak E_s echos, possibly due to extra Na^+ injection during the E_s events, which facilitated additional neutral Na atom formation. The measured nightly averaged temperatures above 100 km (not shown) was also lower with minima of 176 (day 195) and 174 K (day 197), as compared with the average temperatures measured on days 196 (182 K) and 198 (195 K). Based on the early model study by *Plane et al.* [1999], the conversion from Na^+ to Na is a multibody reaction that involves N_2 and other quenching species. One of the key reaction rates is proportional to $\sim 200/T^{2.2}$, indicating that a lower atmospheric temperature would produce a higher Na density above 100 km. This may explain the fact that during the course of E_s, the Na abundance was higher above 105 km, when extra Na^+ injection was combined with a higher conversion rate from Na^+ to Na. However, accurate determination of the top-side mesospheric Na layer changes in association with E_s is still open to question because other possible dynamic or chemical contributions cannot be ruled out at this time. Future coordinated observations, together with a comprehensive modeling study, would be ideal.

4. Discussion

[20] As the geomagnetic activity was mild and stable ($Kp \leq 3$) during the campaign period (data provided by National Oceanic and Atmospheric Administration at http://spidr.ngdc.noaa.gov), indicating quiet solar activity, then the observed E_s perturbations during this time were almost certainly solely driven by atmospheric dynamics. Under these conditions, the "wind shear theory" of E_s formation requires a strong horizontal wind shear, which generates a downward vertical ion drift in the E region. Our results show that the zonal wind shear was mostly driven by tidal wave activity in the mesopause region, and a weakening of the prevailing tidal amplitudes led to the disruption of the conditions for E_s formation.

[21] In our earlier discussions of Figures 5 and 6, we saw that the weakening of the zonal diurnal and semidiurnal tidal winds exhibited a quasi-two-day periodicity, strongly implicating the role of a QTDW in this event. Previously, the QTDW has been measured and shown to introduce significant modulations with periods from 44 to 56 hours in the summer mesosphere [*Salby and Roper*, 1980; *Tsuda et al.*, 1988; *Clark*, 1989; *Clark et al.*, 1994; *Thayaparan et al.*, 1997a, 1997b]. The QTDW is a westward propagating

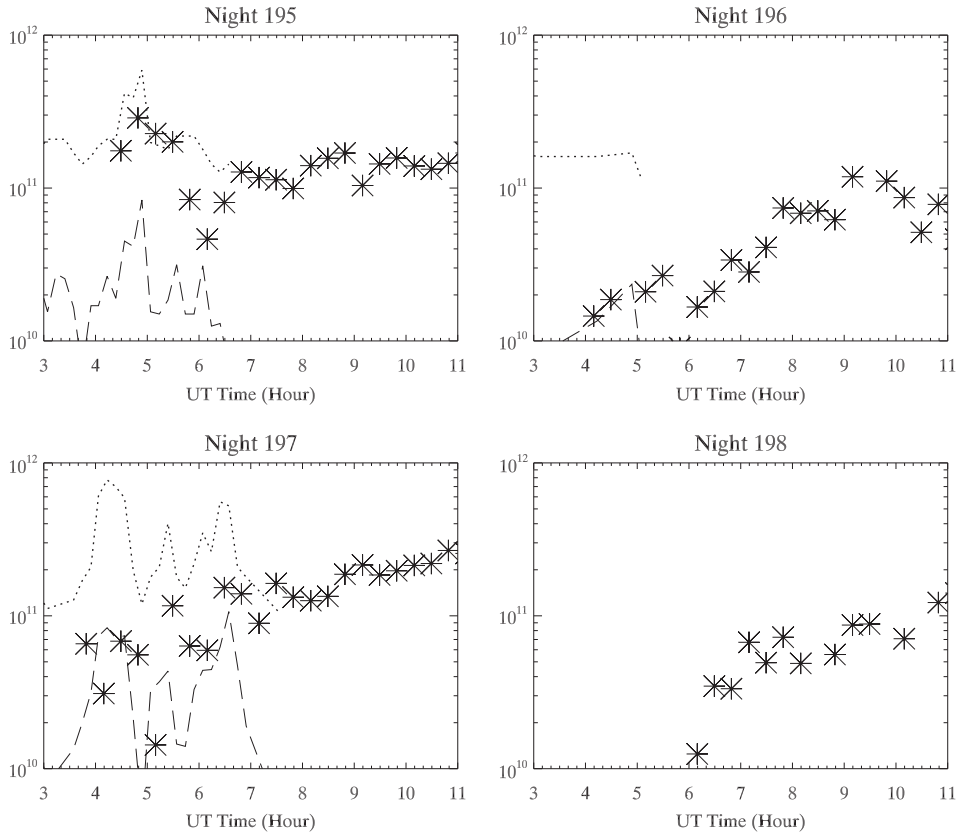

Figure 7. Time series of the Na column abundance (m^{-2}) on the top side of the mesopause region between 105 and 120 km (asterisks) and variations in the E_s and E layer peak electron density (dots) and echo strength (dashes) for the 4 nights of the campaign. The CADI peak electron density are in units of m^{-3}, while the echo strength has been rescaled by a factor of 5.0×10^{10} to fit within the plot).

zonal wavenumber 3 disturbance and typically peaks about 10 days to 2 weeks after the summer solstice. Its sources are believed to be due to the combination of baroclinic-barotropic instabilities and a Rossby wave normal mode [*Palo et al*., 1999; *Yue et al*., 2012]. The appearance of a QTDW can either change the structure of the zonal wind and temperature fields that affect the tidal wave's vertical propagation [*Palo et al*., 1999; *Chang et al*., 2011] or modulates the vertical propagation of GWs, which, in turn, change the wave stress on the tidal waves.

[22] General Circulation Model (GCM) studies have indicated that atmospheric wave-wave nonlinear interactions between a planetary wave and migrating tidal waves [*Palo et al*., 1999] are the most likely cause of significant variations in the tidal wave. When a QTDW occurs, it can decrease the amplitudes of the migrating diurnal and semidiurnal tides. It has been suggested that this decrease in tidal amplitude during the course of such nonlinear interactions can be attributed to nonlinear advection transferring energy from the parent waves (tides and QTDW) to the sum and difference child waves [*Palo et al*., 1998; *Norton and Thuburn*, 1999; *Chang et al*., 2009]. In *Palo et al*.'s [1999] model study, the National Center for Atmospheric Research Thermosphere-Ionosphere-Mesosphere Electrodynamics GCM (TIME-GCM) was forced by the Global Scale Wave Model (?GSWM) [*Hagan et al*., 1999] with a lower boundary (~30 km) for solar thermal tidal inputs. The model simulation indicated a decrease of ~50% for migrating diurnal tides (at low latitudes) and ~40% for the migrating semidiurnal tide (at mid- and high latitude in the summer hemisphere) when QTDW activity was present. The simulation was able to identify that the region where the semidiurnal tidal amplitude experienced most of the reduction resides between 100 and 120 km. This lies right at the lower ionosphere E region where the E_s forms. The damping of migrating diurnal tide, on the other hand, occurs at lower altitudes, near 95 km at low latitudes, which qualitatively explains why the observed diurnal amplitude variations were more significant in the mesopause region than the semidiurnal tide, as measured during the campaign.

[23] Based on our results from the MWR and lidar observations, the theory of tidal wave QTDW nonlinear interaction may also explain the large tidal variability observed by the lidar during the campaign, which contributed to the observed E_s perturbations. As the TIME-GCM model simulations revealed, another consequence of such interactions is the generation of secondary child waves through the sum and difference of both periods and zonal wavenumber of the parent waves (migrating tides and QTDW). This occurs when the parent wave amplitudes become large and the second-order nonlinear effects in the linearized perturbation equations become significant. In fact, the appearance of a 16-hour modulation in the zonal wind periodogram (Figure 4) is predicted in this GCM simulation to be a clear indicator of the existence of a 16-hour child wave generated through such nonlinear wave-wave interactions. However, there are two mechanisms of generating this: One creates a 16-hour wave with a westward wavenumber 4 and is due to the interaction between the migrating diurnal tide and the QTDW, and the other results in a 16-hour wave with an eastward wavenumber 1 through the interaction between the migrating semidiurnal tide and the QTDW and exhibits a much longer vertical wavelength. Observations from a single location, such as our campaign at USU, can determine the generation and the periodicity, but not the full characteristics, of the child wave.

[24] We now investigate the contributions of the various wave components to the total wind shear responsible for the E_s formation. Since all these large-scale waves (QTDW, diurnal, semidiurnal tide, and 16-hour wave) have significant amplitudes in the mesopause region, they may all contribute to the total wind shear in the lower E region. Some previous studies [*Arras et al*., 2009; *Akchurin et al*., 1998] suggest that the semidiurnal tidal component should play dominant role in the mid-latitude E_s due to its large amplitude at mid- and high latitudes. However, to our knowledge, the relative contributions to the wind shear have not been studied in detail, mainly due to lack of coordinated neutral and ionospheric measurements. Equation (3) represents the total zonal wind with contributions from these large-scale global wave modulations, as shown in equation (3):

$$U = \bar{U} + U'_{24} + U'_{12} + U'_{16} + U'_{48} \tag{3}$$

where $\bar{U}$ is mean zonal wind, U'_{24}, U'_{12}, U'_{16}, and U'_{48} are modulations by the diurnal, semidiurnal, 16-hour waves, and the QTDW. Assuming each wave modulation has the form of equation (4),

$$U'_i(z) = A_i(z)\cos(\omega_i t - \varphi_i(z)) \tag{4}$$

where A_i, $\boldsymbol{\omega_I}$, and φ_i are the amplitude, angular velocity, and phase of the wave i. Both amplitude and phase are functions of altitude (z). Thus, the total zonal wind gradient is shown in equation (5).

$$\begin{aligned}\frac{dU}{dz} = \frac{d\bar{U}}{dz} &+ \frac{dA_{24}}{dz}\cos(\omega_{24}t - \varphi_{24}) - A_{24}\sin(\omega_{24}t - \varphi_{24})\frac{d\varphi_{24}}{dz} \\ &+ \frac{dA_{12}}{dz}\cos(\omega_{12}t - \varphi_{12}) - A_{12}\sin(\omega_{12}t - \varphi_{12})\frac{d\varphi_{12}}{dz} \\ &+ \frac{dA_{16}}{dz}\cos(\omega_{16}t - \varphi_{16}) - A_{16}\sin(\omega_{16}t - \varphi_{16})\frac{d\varphi_{16}}{dz} \\ &+ \frac{dA_{48}}{dz}\cos(\omega_{48}t - \varphi_{48}) - A_{48}\sin(\omega_{48}t - \varphi_{48})\frac{d\varphi_{48}}{dz}\end{aligned} \tag{5}$$

[25] Assuming the wave was propagating upward (i.e., downward phase progression) and mode coupling [*Forbes*, 1995] was weak in the lower E region (resulting in a similar vertical wavelength (λ_z) for the tide at the mesopause region and in the E region, between 100 and 120 km), then the vertical gradient of the wave's phase would have been negative with a value of roughly $2\pi/\lambda_z$. For example, on days 195 and 197 when the tides were well defined, then the semidiurnal and diurnal tidal phase vertical gradients would have been $d\varphi_{12}/dz \sim -2\pi/48km$, *and* $d\varphi_{24}/dz \sim -2/20km$, respectively (using the observed λ_z of 48 and 20 km on these nights for the semidiurnal and diurnal tides). This suggests that, even though the diurnal tidal amplitude was less than half of the semidiurnal amplitude near 98 km, the magnitudes of their component terms, $A_{24}\frac{d\varphi_{24}}{dz}$ and $A_{12}\frac{d\varphi_{12}}{dz}$ in equation (3) were, in fact, comparable. In a

separate analysis of the mesopause wind climatology over BLO using imaging Doppler interferometry climatology data (2000–2005) (C. Fish private communication), the diurnal and semidiurnal amplitudes of the zonal and meridional wind components from 100 to 115 were also found to have similar growth rates $\left(\frac{dA_{24}}{dz} \approx \frac{dA_{12}}{dz}\right)$. In an earlier collaborative study on tidal climatology using the Na lidar and the Hamburg Model of the Neutral and Ionized Atmosphere, *Yuan et al*. [2008a, 2008b] with the model showed that the vertical gradient of the zonal wind tidal amplitude between 100 and 115 km was mostly positive and <2 m/s/km during July for both the diurnal and semidiurnal tides. The model also shows that the vertical wavelengths of both the tidal components in the lower E region (100–115 km) do not appear to differ significantly from those in the mesopause region. Together, these results support our above discussion on the vertical gradients of the tidal amplitudes and phases, as their day-to-day variabilities are not expected to differ largely from the model climatology study.

[26] Thus, referring back to equation (3), we see that the first term's contribution of both tidal wave components, which involve the amplitude gradients, are expected to have been much smaller, compared to the second terms and can essentially be neglected. Therefore, both the diurnal and the semidiurnal tidal components could have considerable contributions to the total wind shear in the E_s region, even though diurnal amplitude was less than semidiurnal tide in the mid-latitude mesosphere-lower thermosphere (MLT) region.

[27] Now we consider the QTDW contribution in equation (3). Due to its expected long vertical wavelength (~200 km; *Palo et al*., 1999) and its relatively weak amplitude, compared to the diurnal tide (see Figure 6), the QTDW's second term contribution to the total zonal wind gradient would be insignificant and thus may be neglected. The model simulations have shown that the QTDW can provide enough forcing to the background mean winds to cut off its own growth within the MLT [*Palo et al*., 1998, 1999; *Chang et al*., 2011]. If this situation prevailed, then the first term of the QTDW may also be ignored. Finally, the 16-hour wave's contribution to the total wind shear could be significant due to its comparable amplitude to the tide amplitudes, as revealed by the lidar measurements. However, contrary to the two major tidal components and the QTDW, little is known about the growth rate of the 16-hour wave in the lower E region, nor its vertical wavelength, even though the lidar measurements suggest it was quite long (~36–45 km). The fact that our analysis suggests that it is a child wave resulting from nonlinear interactions between the migrating tide and QTDW seems to suggest that it should exist only in the region where both parent waves' are strong. In the lower E region above 100 km, where the Na lidar data are limited, the QTDW is expected to be much weaker than it is in the mesosphere, and the existence and growth of this 16-hour wave is currently not known. The lidar measurements of 16-hour wave amplitude also suggest its dissipation above 95 km (Figure 3c), making its contribution to the zonal wind shear in lower E region questionable. Thus, it is difficult to estimate its full impacts in the lower E region dynamics at this point and a GCM simulation would be needed to have a clearer understanding on this topic.

5. Summary and Conclusions

[28] Collaborative observations using the Na lidar recently relocated at USU, together with ionosonde and MWR measurements from nearby BLO, have enabled a detailed investigation of the ionospheric E_s formation and evolution at mid-latitudes over a continuous 4-day period during July 2011. The lidar provided high resolution data on the Na density and atmospheric dynamical parameters, including neutral temperature, horizontal winds, and the amplitudes of the prevailing tidal perturbations, which were critical for investigating the formation and propagation of the E_s layer through the lower E region. The results of this investigation are summarized as follows:

[29] (1) The ionosonde detected a weakening in the descending E layer echoes observed on two days (196 and 198) coincident with a large reduction in the zonal diurnal and semidiurnal amplitudes above 95 km, as measured by both the lidar and the MWR.

[30] (2) The weakening of the diurnal and semidiurnal amplitude, as well as the disruption in the vertical propagation of the tidal waves associated with significant QTDW activity above 92 km, as revealed by MWR data.

[31] (3) A 16-hour wave was detected in all fields on days 195 and 197 with comparable amplitudes to the tidal waves.

[32] (4) On days of strong E_s (195 and 197), large modulations of the top-side mesospheric Na layer (above 105 km) occurred, which were synchronized with strong oscillations in the ionosonde E region echoes.

[33] (5) Compared with the strong E_s days, the observed weakening of the ionosonde echoes on days 196 and 198 were associated with decreasing Na abundance and warmer mean nocturnal temperatures in the upper mesopause region (above 100 km).

[34] The appearance of both a QTDW and a 16-hour modulation in the lidar measured zonal wind fields (and the MWR data, not shown), indicates that a strong wave-wave nonlinear interaction occurred between tidal wave and QTDW. Based on earlier TIME-GCM simulations, these interactions can cause damping of the migrating tidal wave amplitude and disruption of the tidal waves' vertical propagation. Since migrating tides are the dominant tidal components near 41°N [*Yuan et al*., 2006, 2008a], and tidal wave modulations are major drivers of the lower E region dynamics, the overall effect was that of disturbing the formation of the large vertical zonal wind shear, which is critical for E_s formation and its downward propagation. Further detailed analysis suggests that, although the diurnal amplitude was smaller than the semidiurnal component, its contributions to the total wind shear in the lower E region was probably comparable to the semidiurnal tide, due to its shorter vertical wavelength, and thus the diurnal tidal effects should not be ignored in future mid-latitude E_s studies. Our results also show that the 16-hour child wave could make significant contributions to the total wind shear in the lower E region, but this interaction needs further investigation and modeling to determine its impact on the E_s formation. In contrast, the QTDW does not appear to contribute directly to the wind shear very much due to its long vertical wavelength and its rather small amplitude. However, the QTDW is indirectly involved in the E_s formation and propagation in the lower E region ionosphere through its modulations

of the tidal waves and the generation of the child. Finally, the lidar observed disturbance within the top-side Na layer was most likely due to the injection of additional electrons and Na^+ atoms from the descending E_s into the top of the mesopause region that disturbed the formation of atomic Na within the lower E region. This study provides new direct evidence that tidal and planetary waves generated in the lower atmosphere can significantly affect the E region ionospheric dynamics.

[35] **Acknowledgments.** This study was performed as part of a collaborative research program supported under the Consortium of Resonance and Rayleigh Lidars National Science Foundation (NSF) Grant 1135882, with additional support from NSF grants AGS-1041571 and AGS-0962544. BLO instrument operations are supported, in part, by the Center for Atmospheric and Space Sciences and the Space Dynamics Laboratory at USU. The SkiYMet MWR was operated at BLO in collaboration with N.J. Mitchell at The University of Bath (Bath,UK) under a Natural Environment Research Council grant (NE/H009760/1). The CADI operations at BLO were supported by the SEC.

References

Akchurin, A. D., E. Yu. Zykov, N. A. Makarov, R. G. Minullin, Yu. A. Portnyagin, and O. N. Sherstyukov (1998), The influence of the semidiurnal tide on altitude variations of the sporadic E layer, *Int. J. Geomag. Aeronom.*, *1*(1), doi:10.1016/S0273-1177(97)00679-0.

Arras, C., C. Jacobi, and J. Wickert (2009), Semidiurnal tidal signature in sporadic E occurrence rates derived from GPS radio occultation measurements at higher midlatitudes, *Ann. Geophys.*, *27*, 2555–2563, doi:10.5194/angeo-27-2555-2009.

Chang, L. C., S. E. Palo, and H.-L. Liu (2011), Short-term variability in the migrating diurnal tide caused by interactions with the quasi 2 day wave, *J. Geophys. Res.*, *116*, D12112, doi:10.1029/2010JD014996.

Chang, L. C., S. E. Palo, and H.-L. Liu (2009), Short-term variation of the s = 1 nonmigrating semidiurnal tide during the 2002 stratospheric sudden warming, *J. Geophys. Res.*, *114*, D03109, doi:10.1029/2008JD010886.

Chen, H., M. A. White, D. A. Krueger, and C. Y. She (1996), Daytime mesopause temperature measurements using a sodium-vapor dispersive Faraday filter in lidar receiver, *Opt. Lett.*, *21*, 1003–1005, doi:10.1364/OL.21.001093.

Clark, R. R., A. C. Current, A. H. Manson, C. E. Meek, S. K. Avery, S. E. Palo, and T. Aso (1994), Hemispheric properties of the two-day wave from mesosphere-lower thermosphere radar observation, *J. Atmos. Terr. Phys.*, *59*, 1279–1288, doi:10.1016/0021-9169(94)90066-3.

Clark, R. R. (1989), The quasi 2-day wave at Durham (43°N): Solar magnetic effects, *J. Atmos. Sci.*, *51*, 617–622, doi:10.1016/0021-9169(89)90059-7.

Forbes, J. M. (1995), Tidal and planetary waves, in The Upper Mesosphere and Lower Thermosphere: A Review of Experiment and Theory, Geophys. Monogr. Ser., vol. 87, edited by R. M. Johnson and T. L. Killeen, pp. 67–87, AGU, Washington, D. C.

Hagan, M. E., R. G. Burrage, J. M. Forbes, H. Hackney, W. J. Randel, and X. Zhang (1999), GSWM-98: Results for migrating solar tides, *J. Geophys. Res.*, *104*, 6813–6828, doi:10.1029/1998JA900125.

Haldoupis, C., D. Pancheva, W. Singer, C. Meek, and J. MacDougall (2007), An explanation for the seasonal dependence of midlatitude sporadic E layers, *J. Geophys. Res.*, *112*, A06315, doi:10.1029/2007JA012322.

Haldoupis, C., D. Pancheva, and N. J. Mitchell (2004), A study of tidal and planetary wave periodicities present in midlatitude sporadic E layers, *J. Geophys. Res.*, *109*, A02302, doi:10.1029/2003JA010253.

Haldoupis, C., and D. Pancheva (2002), Planetary waves and midlatitude sporadic E layers: Strong experimental evidence for a close relationship, *J. Geophys. Res.*, *107*(A6), 1078, doi:10.1029/2001JA000212.

Hocking, W. K., B. Fuller, and B. Vandepeer (2001), Real-time determination of meteor-related parameters utilizing modern digital technology, *J. Atmos. Solar-Terr. Phys. 63*, 155–169, doi:10.1016/S1364-6826(00)00138-3.

Lanchester, B. S., T. Nygrén, A. Huuskonen, T. Turunen, and M. J. Jarvis (1991), Sporadic-E as a tracer for atmospheric waves, *Plan. Space Sci.*, *39*, 1421–1434. doi:10.1016/0032-0633(91)90021-2.

Li, F., A. Z. Liu, and G. R. Swenson (2005a), Characteristics of instabilities in the mesopause region over Maui, Hawaii, *J. Geophys. Res.*, *110*, D09S12, doi:10.1029/2004JD005097.

Li, F., A. Z. Liu, G. R. Swenson, J. H. Hecht, and W. A. Robinson (2005b), Observations of gravity wave breakdown into ripples associated with dynamical instabilities, *J. Geophys. Res.*, *110*, D09S11, doi:10.1029/2004JD004849.

Liu, H.-L. (2007), On the large wind shear and fast meridional transport above the mesopause, *Geophys. Res. Lett.*, *34*, L08815, doi:10.1029/2006GL028789.

Mathews J. D. (1998), Review paper: Sporadic E: current views and recent progress, *J. Atmos. Solar-Terr. Phys.*, *60*, 413–435, doi:10.1016/S1364-6826(97)00043-6.

McCormack, J. P., S. D. Eckermann, K. W. Hoppel, and R. A. Vincent (2010), Amplification of the quasi-two day wave through nonlinear interaction with the migrating diurnal tide, *Geophys. Res. Lett.*, *37*, L16810, doi:10.1029/2010GL043906.

Norton, W. A., and J. Thuburn (1999), Sensitivity of mesospheric mean flow, planetary waves, and tides to strength of gravity wave drag, *J. Geophys. Res.*, *104*(D24), 30,897–30,911, doi:10.1029/1999JD900961.

Palo, S. E., R. G. Roble, and M. E. Hagan (1999), Middle atmosphere effects of the quasi-two-day wave determined from a General Circulation Model, *Earth Planets Space*, *51*, 629–647.

Palo, S. E., R. G. Roble, and M. E. Hagan (1998), TIME-GCM results for the quasi-two-day wave, *Geophys. Res. Lett.*, *25*(20), 3783–3786, doi:10.1029/1998GL900032.

Plane, J. M., C. S. Gardner, J. Yu, C. Y. She, R. R. Garcia, and H. C. Pumphrey (1999), Mesospheric Na layer at 40 N: Modeling and observations, *J. Geophys. Res.*, *104*(D3), 3773–3788, doi:10.1029/1998JD100015.

Raizada, S., C. A. Tepley, N. Aponte, and E. Cabassa (2011), Characteristics of neutral calcium and Ca^+ near the mesopause, and their relationship with sporadic ion/electron layers at Arecibo, *Geophys. Res. Lett.*, *38*, L09103, doi:10.1029/2011GL047327.

Salby, M. L., and R. G. Roper (1980), Long-period oscillations in the meteor region, *J. Atmos. Sci.*, *37*, 237–244, doi:10.1175/1520-0469(1980)037 < 0237:LPOITM > 2.0.CO;2.

She, C. Y., et al. (2004), Tidal perturbations and variability in the mesopause region over Fort Collins, CO (41°N, 105°W): Continuous multi-day temperature and wind lidar observations, *Geophys. Res. Lett.*, *31*, L24111, doi:10.1029/2004GL021165.

Tepley, C. A., S. Raizada, Q. Zhou, and J. S. Friedman (2003), First simultaneous observations of Ca+, K, and electron density using lidar and incoherent scatter radar at Arecibo, *Geophys. Res. Lett.*, *30*(1), 1009, doi:10.1029/2002GL015927.

Thayaparan, T., W. K. Hocking, and J. MacDougall (1997a), Amplitude, phase, and period variations of the quasi 2-day wave in the mesosphere and lower thermosphere over London, Canada (43°N, 81°W), during 1993 and 1994, *J. Geophys. Res.*, *102*(D8), 9461–9478, doi:10.1029/96JD03869.

Thayaparan, T., W. K. Hocking, J. MacDougal, A. H. Manson, and C. E. Meek (1997b), Simultaneous observations of the 2-day wave at London Ontario (43°N, 81°W) and Saskatoon (52°N, 107° W) near 91 km altitude during the two years 1993 and 1994, *Ann. Geophys.*, *15*, 1324–1339, doi:10.1007/s00585-997-1324-3.

Tong, Y., J. D. Mathews, and W.-P. Ying (1988), An upper E region quarterdiurnal tide at Arecibo?, *J. Geophys. Res.*, *93*(A9), 10,047–10,051, doi:10.1029/JA093iA09p10047.

Tsuda, T., S. Kato, and R. A. Vincent (1988), Long period wind oscillations observed by the Kyoto meteor radar and comparisons of the quasi-2-day wave with Adelaide HF radar observations, *J. Atmos. Terr. Phys.*, *50*, 225–230, doi:10.1016/0021-9169(88)90071-2.

Voiculescu, M., C. Haldoupis, D. Pancheva, M. Ignat, K. Schlegel, and S. Shalimov (2000), More evidence for a planetary wave link with midlatitude E region coherent backscatter and sporadic E layers, *Ann. Geophys.*, *18*, 1182–1196, doi:10.1007/s00585-000-1182-8.

Whitehead, J. D. (1989), Recent work on mid-latitude and equatorial sporadic E, *J. Atmos. Terr. Phys.*, *51*, 401–424, doi:10.1016/0021-9169(89)90122-0.

Williams, B. P., J. Sherman, C. Y. She, and F. T. Berkey (2007), Coincident extremely large sporadic sodium and sporadic E layers observed in the lower thermosphere over Colorado and Utah, *Ann. Geophys.*, *25*, 3–8, doi:10.5194/angeo-25-3-2007.

Yuan, T., C. Y. She, J. Forbes, X. Zhang, D. Krueger, and S. Reising (2010), A collaborative study on temperature diurnal tide in the midlatitude mesopause region (41°N, 105°W) with Na lidar and TIMED/SABER observations, *J. Atmos. Solar-Terr. Phys. 72*, 541–549, doi:10.1016/j.jastp.2010.06.012.

Yuan, T., H. Schmidt, C. Y. She, D. A. Krueger, and S. Reising (2008a), Seasonal variations of semidiurnal tidal perturbations in mesopause region temperature and zonal and meridional winds above Fort Collins, Colorado (40.6°N, 105.1°W), *J. Geophys. Res.*, *113*, D20103, doi:10.1029/2007JD009687.

Yuan, T., C.-Y. She, D. A. Krueger, F. Sassi, R. Garcia, R. G. Roble, H.-L. Liu, and H. Schmidt (2008b), Climatology of mesopause region temperature, zonal wind, and meridional wind over Fort Collins, Colorado (41°N, 105°W), and comparison with model simulations, *J. Geophys. Res.*, *113*, D03105, doi:10.1029/2007JD008697.

Yuan, T., et al. (2006), Seasonal variation of diurnal perturbations in mesopause region temperature, zonal, and meridional winds above Fort Collins, Colorado (40.6°N, 105°), *J. Geophys. Res. 111*, D06103, doi:10.1029/2004JD005486.

Yue, J., H.-L. Liu, and L. C. Chang (2012), Numerical investigation of the quasi 2 day wave in the mesosphere and lower thermosphere, *J. Geophys. Res.*, *117*, D05111, doi:10.1029/2011JD016574.

Yue, J., C.-Y. She, and H.-L. Liu (2010), Large wind shears and stabilities in the mesopause region observed by Na wind-temperature lidar at midlatitude, *J. Geophys. Res.*, *115*, A10307, doi:10.1029/2009JA014864.

Zhao, Y., A. Z. Liu, and C. S. Gardner (2003), Measurements of atmospheric stability in the mesopause region at Starfire Optical Range, NM, *J. Terr. Sol. Atmos. Phys.*, *65*, 219–232, doi:10.1016/S1364-6826(02)00288-2.

Zeng, Z., and S. Sokolovskiy (2010), Effect of sporadic E clouds on GPS radio occultation signals, *Geophys. Res. Lett.*, *37*, L18817, doi:10.1029/2010GL044561.